Bioactive Materials 6 (2021) 1988–1999

Contents lists available at ScienceDirect

Bioactive Materials

journal homepage: www.sciencedirect.com/journal/bioactive-materials

Injectable silk sericin scaffolds with programmable shape-memory property and neuro-differentiation-promoting activity for individualized brain repair of severe ischemic stroke

Jian Wang [a,b], Xiaolin Li [b], Yu Song [b], Qiangfei Su [b], Xiakeerzhati Xiaohalati [b], Wen Yang [b], Luming Xu [b], Bo Cai [b], Guobin Wang [c,***], Zheng Wang [b,c,**], Lin Wang [a,b,*]

[a] Department of Clinical Laboratory, Union Hospital, Tongji Medical College, Huazhong University of Science and Technology, Wuhan, 430022, China
[b] Research Center for Tissue Engineering and Regenerative Medicine, Union Hospital, Tongji Medical College, Huazhong University of Science and Technology, Wuhan, 430022, China
[c] Department of Gastrointestinal Surgery, Union Hospital, Tongji Medical College, Huazhong University of Science and Technology, Wuhan, 430022, China

ARTICLE INFO

Keywords:
Stroke cavities
Silk sericin scaffolds
Shape-memory properties
Injectability
Neuronal differentiation

ABSTRACT

Severe ischemic stroke damages neuronal tissue, forming irregular-shaped stroke cavities devoid of supporting structure. Implanting biomaterials to provide structural and functional support is thought to favor ingrowth of regenerated neuronal networks. Injectable hydrogels capable of *in situ* gelation are often utilized for stroke repair, but challenged by incomplete gelation and imprecise control over end-macrostructure. Injectable shape-memory scaffolds might overcome these limitations, but are not explored for stroke repair. Here, we report an injectable, photoluminescent, carbon-nanotubes-doped sericin scaffold (CNTs-SS) with programmable shape-memory property. By adjusting CNTs' concentrations, CNTs-SS′ recovery dynamics can be mathematically calculated at the scale of seconds, and its shapes can be pre-designed to precisely match any irregular-shaped cavities. Using a preclinical stroke model, we show that CNTs-SS with the customized shape is successfully injected into the cavity and recovers its pre-designed shape to well fit the cavity. Notably, CNTs-SS' near-infrared photoluminescence enables non-invasive, real-time tracking after *in vivo* implantation. Moreover, as a cell carrier, CNTs-SS not only deliver bone marrow mesenchymal stem cells (BMSCs) into brain tissues, but also functionally promote their neuronal differentiation. Together, we for the first time demonstrate the feasibility of applying injectable shape-memory scaffolds for stroke repair, paving the way for personalized stroke repair.

1. Introduction

Severe ischemic stroke causes neuronal tissue damage, leading to severe disabilities greatly affecting patients' quality of life [1,2]. Stroke often results in irregular-shaped cavities that are filled with extracellular fluid (ECF), but lack supporting structure [3,4]. Currently, no therapies can effectively reverse stroke-induced brain damages [5], largely due to severely limited endogenous neuronal regenerative capability and cavitary harsh microenvironment. Implanting biomaterials to provide extracellular matrix and structural support is thought to facilitate endogenous or implanted stem cells forming *de novo* neuronal circuit networks [6,7].

Several injectable hydrogels capable of *in situ* gelation, such as hyaluronic acid (HA) hydrogels [8], plasma gels [9], Matrigel [10], microporous particle hydrogels [11], and extracellular matrix (ECM) hydrogels [3], have been previously studied for stroke repair. Some of these injectable hydrogels have been shown to reduce lesion volume and promote angiogenesis and neurogenesis after approximately 3–40 μL of them are implanted into rodent stroke cavity [3,7,9]. However, as for stroke lesion volume, it ranges from 2 mL to 200 mL in human [12,13], much larger than that in rodent stroke models. Thus, it is difficult for the stroke cavity (filled with ECF) to further accommodate the volume of

Peer review under responsibility of KeAi Communications Co., Ltd.
* Corresponding author. Huazhong University of Science and Technology, Wuhan, 430022, China.
** Corresponding author. Huazhong University of Science and Technology, Wuhan, 430022, China.
*** Corresponding author.
E-mail addresses: wgb@hust.edu.cn (G. Wang), zhengwang@hust.edu.cn (Z. Wang), lin_wang@hust.edu.cn (L. Wang).

https://doi.org/10.1016/j.bioactmat.2020.12.017
Received 28 October 2020; Received in revised form 12 December 2020; Accepted 20 December 2020

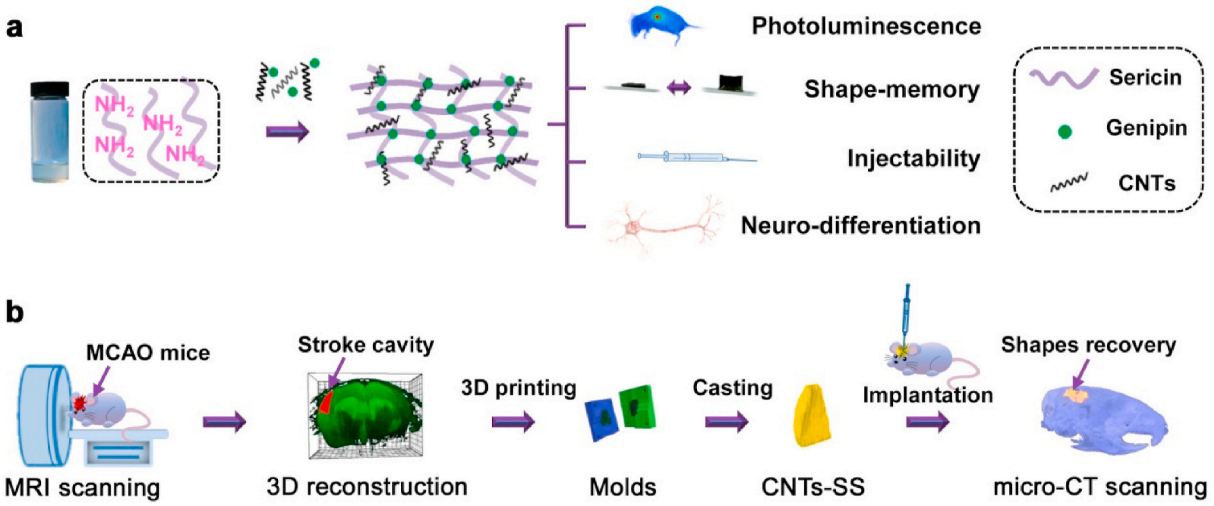

Scheme 1. (a) Schematics showing the design and the main properties of CNTs-SS. (b) Schematics of the application of CNTs-SS in filling stroke cavities for brain tissue repair.

hydrogel precursor solutions for forming a repairing hydrogel. Meanwhile, these hydrogels are challenged by their limited control over end-shapes/macrostructures. Injectable hydrogels are commonly delivered by local injection of liquid precursor solutions [14]. During subsequent *in situ* gelation, dilution of precursor solutions with the pre-existing ECF in stroke cavities and their leakage into cerebral ventricles often lead to incomplete gelation or results in geometrically and mechanically unpredictable end-macrostructures [15]. These would make hydrogels either fail to effectively support/contact with the cavitary wall (a site with the highest neuronal plasticity after stroke), or produce excessive pressure compressing peri-cavitary normal brain tissue [16]. To overcome these challenges, we proposed to utilize injectable, shape-memory scaffolds. This type of scaffolds can be readily compressed into small volumetric grafts conveniently injected into stroke cavities, followed by ECF-triggered restoration to their original geometries that were designed to well match irregular-shaped cavities, where the scaffolds supply artificial extracellular matrix and appropriate structural support to promote brain tissue regeneration. Meanwhile, as stem cells are key to brain regeneration [17,18], it would be ideal if shape-memory scaffolds for stroke repair were also able to effectively deliver stem cells to brain, protect them from pathophysiologically hostile cavitary conditions, and promote their differentiation towards neurons for neuronal network regeneration.

Here, we report the design and fabrication of an injectable, photoluminescent, carbon-nanotubes (CNTs)-doped silkworm sericin (a major component of silkworm silk fibers) scaffold (SS) as a cell carrier for repair of stroke-affected brain. Innovative doping of CNTs into a sericin hydrogel conferred this composite scaffold (CNTs-SS) (Scheme 1a) with mathematically programmable shape-memory property, where deformation recovery dynamics could be controlled at the time scale of seconds. To precisely guide the fabrication of CNTs-SS, we three-dimensionally reconstructed MRI images of stroke cavities in an ischemic stroke model mouse (middle cerebral artery occlusion, MCAO) to generate a 3D-printed mold for casting individualized CNTs-SS with geometries matching a given irregular-shaped cavity (Scheme 1b). Using this MCAO stroke mouse model [19], we demonstrated that the cast CNTs-SS was successfully injected into the cavity and effectively restored its pre-designed shape fitting the cavity *in vivo*. Moreover, silk sericin's natural cell-adhesiveness and unique neuro-protective activity in conjunction with CNTs' reportedly neuro-differentiation-promoting activity [20–24], enhanced infiltration of carried stem cells into surrounding brain tissues, and more importantly, molecularly activated these stem cells to differentiate towards neurons. This work demonstrates the suitability and potentiality of CNTs-SS material for minimally invasive repair of severe ischemic stroke, providing experimental evidence for its potential clinical translational utilization.

2. Materials and methods

2.1. Materials

The mutant silkworm cocoons (*Bombyx mori,* 140 Nd-*s*) were provided by the Sericultural Research Institute, China Academy of Agricultural Sciences (Zhenjiang, Jiangsu, China). Carboxyl acid group functionalized multiwalled CNTs were purchased from XFNANO (Nanjing, China). LiBr was purchased from Sigma-Aldrich (USA). Live-&Dead cell staining kits were purchased from Biovision (USA).

2.2. Preparation of CNTs-SS

Sericin was extracted from fibroin-deficient silkworm cocoons, *Bombyx mori,* 140 Nd-*s*, using LiBr isolation method as previously described [20]. These mutant silkworm cocoons are mainly composed of sericin. A gram of CNTs was added into 10 mL distilled water. After sonication for 30 min, the dispersed CNTs solution (10%, *w/v*; distilled water) was prepared. 200 μL genipin (1%, *w/v*; distilled water) was added into 1.2 mL sericin solution (2%, *w/v*; distilled water) to prepare the precursor solution. The dispersed CNTs solution and the precursor solution were thoroughly mixed at various volume ratios. After gelation and lyophilization, the CNTs-SS with different CNTs concentrations were prepared.

2.3. Characterizations of physical properties

The surfaces of the CNTs-SS were examined by a scanning electron microscope (SEM; SM-5610LV, Japan) with 25 kV working voltage. The pore sizes of different specimens were analyzed by ImageJ software. The mechanical properties of CNTs-SS were examined by a universal testing machine (Instron 5848 MicroTester, USA) equipped with a 100 N load cell. The dynamic swelling behaviors of the CNTs-SS were examined as previously described [20]. Briefly, CNTs-SS were immersed in phosphate-buffered saline (PBS) at 37 °C for 10 days. The dry weight (W_d) and swollen weight (W_s) of the scaffolds at a specified time point were recorded and the swelling ratios were calculated by following equation: Swelling (%) = $(W_s - W_d)/(W_d) \times 100\%$.

2.4. Cell culture

Bone marrow mesenchymal stem cells (BMSCs) were isolated from wild-type mice or GFP transgenic mice as previously reported [25]. Briefly, Iscove's Modified Dulbecco's Medium (IMDM, Hyclone, UT, USA) was infused into femurs and tibia lumens to flush marrow. The marrow was placed in a tissue culture flask. After a 3-day incubation, the unattached cells were removed. The adherent cells were cultured in IMDM supplemented with 10% fetal bovine serum (FBS, Gibco, CA, USA) and 1% penicillin-streptomycin (Hyclone, UT, USA). After 5 passages, the BMSCs were used for experiments. SHSY-5Y cells or GFP-expressing SHSY-5Y cells were cultured in complete Dulbecco Modified Eagle Medium (DMEM, Hyclone, UT, USA) supplemented with 10% FBS and 1% penicillin-streptomycin. All cells were incubated in a humidified incubator at 37 °C with 5% CO_2.

2.5. Seeding cells on prepared scaffolds

The CNTs-SS were sterilized by immersion in 75% ethanol for 1 h and washed with PBS to remove residual ethanol. Then 2×10^5 cells (SHSY–5Y or BMSCs) were digested and suspended in 50 μL basal medium. The cell suspension was seeded on the top surface of the scaffold with 10 μL at 4 peripheral points and 10 μL at the central point. The cells in the scaffolds were cultured in corresponding medium at 37 °C with 5% CO_2.

2.6. Analysis of cell morphology and viability

To view cell adhesion, extension and growth, the GFP-expressing cells (SHSY–5Y or BMSCs) cultured in CNTs-SS were imaged using a confocal laser scanning microscope (Nikon A1Si, Japan) according to our previous study [21]. For CCK-8 assay (Dojindo, Japan), SHSY-5Y cells (5000 cells per well) were seeded in a 96-well plate coated with SS (control) or CNTs-SS. After a 3-day culture, a total of 100 μL DMEM mixed with 10 μL CCK-8 solution was added into each well and incubated for 45 min at 37 °C. The absorbance was measured at 450 nm using a microplate reader (TECAN, Mannedorf, Switzerland). The Live&Dead cell staining was performed as previously described [21]. Briefly, SHSY-5Y cells in CNTs-SS were digested and incubated with staining solution for 15 min at 37 °C. Then the cells were subject to analysis using a FACSCalibur flow cytometer (BD Canto II, NJ, USA).

2.7. In vivo biocompatibility

All animal experimental protocols were approved by the Animal Care and Use Committee, Tongji Medical College, Huazhong University of Science and Technology (Wuhan, China). The C57BL/6J mice were anesthetized and a hole with a 4-mm diameter was drilled in the skull. Disk-shaped CNTs-SS with a diameter of 3 mm were implanted onto exposed brain surface of mice. After 14 days, the mice were anesthetized, perfused with 0.9% NaCl (*w/v*, distilled water) and then fixed with 4% paraformaldehyde (*w/v*, PBS). The fixed brains were embedded in paraffin and cut into 5-μm sections for immunofluorescence staining. The rabbit anti-mouse GFAP (1:100 diluted; BA0056, Boster, Wuhan, China) and rabbit anti-mouse IBA-1 (1:200 diluted; Ab178847, Abcam, MA, USA) were used to detect astrocytes and microglia, respectively.

2.8. Biodegradation

To test *in vivo* degradation of CNTs-SS, disk-shaped CNTs-SS with a 3-mm diameter were implanted onto the surface of exposed murine brain. At the indicated time point, the mice were sacrificed. Then, the scaffolds were taken out and dried for weighing (W_n). The initial weight (W_0) of CNTs-SS was recorded and the residual weight percentages were calculated by the following equation: Residual weight (%) $= W_n / W_0 \times 100\%$.

2.9. Analysis of cell migration from CNTs-SS in vivo

GFP-expressing BMSCs were seeded in a disk-shaped CNTs-SS with a 3-mm diameter and cultured for 3 days. Then the scaffolds carrying GFP-expressing BMSCs were implanted onto the surface of exposed murine brain. After 7 or 14 days, the mice were anesthetized, perfused with 0.9% NaCl (*w/v*, distilled water) and then fixed with 4% paraformaldehyde (*w/v*, PBS). The fixed brains were embedded in paraffin and cut into 5-μm sections. After being stained with 4',6-diamidino-2-phenylindole (DAPI, Sigma, TX, USA) and Tuj1 antibody (1:100 diluted; Ab52623, Abcam, MA, USA), the brain sections were observed using an inverted fluorescence microscope (Olympus IX71, Japan).

2.10. Characterization of shape-memory property

The T-shaped, I-shaped and pentagram-shaped CNTs-SS were fabricated by mold casting. The scaffolds were immersed in PBS for 30 min and subjected to compression and rehydration in PBS. The compressed scaffolds and rehydrated scaffolds were imaged using a camera (Sony ILCE, Japan). For mathematical model establishment, a series of cubic CNTs-SS (10 mm × 10 mm × 10 mm) were fabricated. The scaffold was immersed in PBS for 30 min and then compressed into a square-shaped small graft. PBS was continuously dripped onto the scaffold and the video was captured. The images were extracted from the video and analyzed by ImageJ software. Multiple linear regression was performed to establish the mathematical model using MATLAB software (VisionR2012b, MathWorks, MA, USA). For *in vivo* experiments, a pentagram-shaped CNTs-SS was fabricated and compressed. After a C57BL/6J mouse was anesthetized, a 1-mm incision was opened on the abdomen and the compressed scaffold was implanted through the incision. The images were continuously captured by a versatile small animal imaging system (In-Vivo FX PRO, Bruker, Germany).

2.11. Characterization of injectability

The CNTs-SS were fabricated in three different shapes, including a 4 mm × 4 mm square shape, a 6 mm × 6 mm square shape and a 3-mm-diameter disk shape. After being immersed in PBS for 30 min, the scaffolds were suspended in 0.3 mL PBS and injected by a syringe through a 16G needle. During injection, the videos and the images were captured. For *in vivo* injection experiments, disk-shaped CNTs-SS were suspended in 0.3 mL PBS and then injected into different sites of mice, including skin, muscle, abdomen and brain, through a 16G needle. The mice were anesthetized and imaged using a versatile small animal imaging system. The mice receiving a subcutaneous injection of the scaffold were imaged by a camera. To test cell viability after injection, confocal laser imaging and the Live&Dead cell staining were performed. GFP-expressing SHSY-5Y cells or wild-type SHSY-5Y cells were seeded in the disk-shaped CNTs-SS and cultured for 24 h. After being injected through a 16G needle, the scaffolds loaded with cells were cultured for another 24 h. The non-injected scaffolds were set as a control. Then the scaffolds loaded with GFP-expressing SHSY-5Y cells were observed under a confocal laser scanning microscope. The wild-type SHSY-5Y cells in the scaffolds were digested and subjected to Live&Dead cell staining.

2.12. In vitro implantation of CNTs-SS into PDMS cavity

Polydimethylsiloxane (PDMS) precursor (A) and crosslinker (B) were mixed at the ratio of 10:1. The mixture was poured into a 1.5 cm × 1.5 cm square-shaped mold. After being cured at 110 °C for 30 min, a piece of square-shaped PDMS was fabricated. Then a hole with a 3-mm diameter was punched at the centre of the PDMS. After being treated with oxygen PLASMA (PDC-32G-2, Harrick, USA), the punched PDMS was bonded to two pieces of un-punched PDMS to obtain a PDMS cavity. Three disk-shaped CNTs-SS were compressed into small grafts, loaded

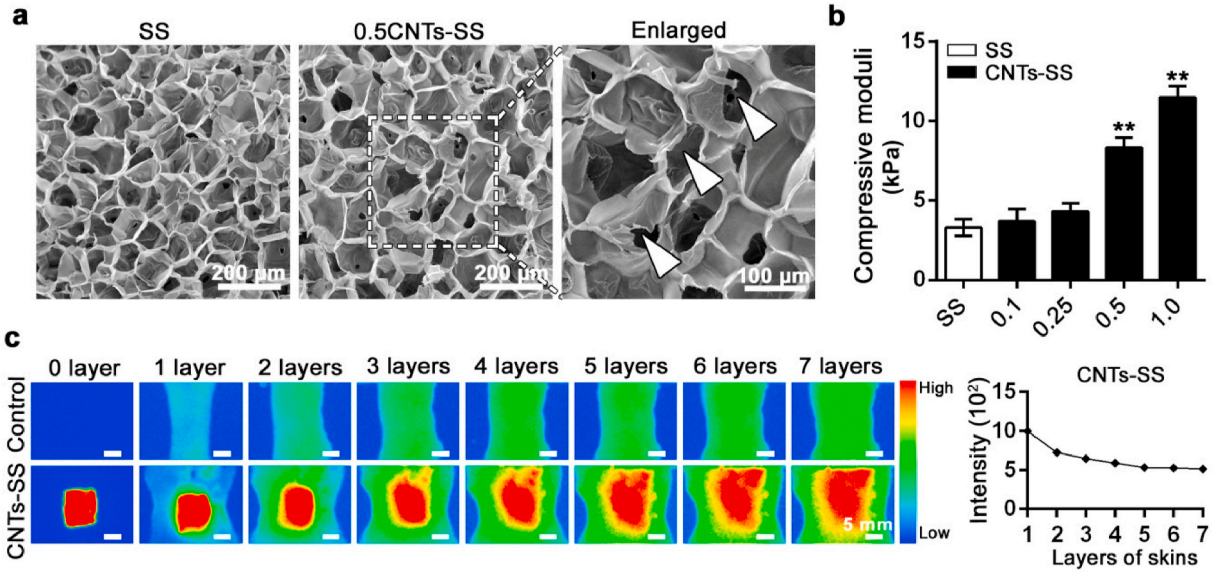

Fig. 1. Characterizations of the CNTs-SS. (a) Scanning electron microscopy (SEM) images of SS and 0.5CNTs-SS. The region boxed with white dashed lines was enlarged on the right with white arrowheads indicating interconnected pores. (b) The compressive moduli of SS (control) and CNTs-SS with different CNTs' concentrations. **, $P < 0.01$; ANOVA. (c) Fluorescent images (left) and quantification (right) of the fluorescence emitted from 0.5CNTs-SS under layers (1–7) of murine skins. The images were captured by a small animal imaging system (excitation 700 nm; emission 750 nm). Murine skin alone was imaged as the control.

into the tip of a 16G flat-head needle, and then vertically, obliquely, or horizontally injected into the three PBS-filled PDMS cavities, respectively. All of these PDMS cavities were imaged before, during and after injection.

2.13. *In vivo application of a customizable CNTs-SS for filling stroke cavities*

The C57BL/6J mice were subjected to transient focal cerebral ischemia by middle cerebral artery blockade (MCAO) with a suture as previously described [19]. After 2 weeks, the MCAO mouse's brain was imaged using a magnetic resonance imaging (MRI) system. Using surface rendering and fluorescence thresholding in Imaris software, the MRI images of the stroke cavity were three-dimensionally reconstructed. The 3D images of stroke cavity were converted to STL-format files for designing 3D molds (RAYDATA, Wuhan, China). Then the corresponding 3D molds were printed by a 3D printer (Phoenix Touch Pro, S-MARKER, China). The CNTs-SS with customized shapes were fabricated through casting in these molds. To visualize the scaffolds in micro-CT scanning, the CNTs-SS were mixed with 0.1% $BaSO_4$ during fabrication. The MCAO mouse was anesthetized and the skull was drilled. The scaffold was compressed, loaded in the tip of a 16G flat-head needle, and transplanted into the stroke cavity by stereotactic injection. Then the mouse was scanned by a Skyscan 1176 micro-CT (Bruker, Germany).

2.14. *Construction of TPIS (Tuj1 promoting imaging system)*

The Tuj1 promoter sequence was cloned from the genomic DNA of the C57BL/6J mouse brain tissue. The promoter region spanning 2900 bp upstream of Tuj1 starting codon ATG was cloned using the following primers: forward, 5′-GATACTAGTCTAAGGGGGAGCAACT-3'; reverse, 5′-TCGAATTCGCTGACTTCACGCGGCT-3'. The restriction enzyme sites (*Spe*I and *Eco*RI, underlined) were designed into these primers. The Tuj1 promoter sequence was inserted into a pCDH vector (System Biosciences, CA, USA) to replace the MSCV promoter sequence on the backbone. The mCherry coding sequence (CDS) was cloned from a px330-mCherry vector (Addgene 98,750, USA) using the following primers [26]: forward, 5′-GCGAATTCATGGTGAGCAAGGGCGA-3'; reverse, 5′-GCGGATCC TTACTTGTACAGCTCGT-3'. The restriction enzyme sites (*Eco*RI and *Bam*HI, underlined) were designed into these primers. The mCherry CDS sequence was inserted into the pCDH vector backbone downstream of the Tuj1 promoter sequence to yield the pTuj1-mCherry vector. GFP expression was driven by the EF1α promoter independently within the vector.

2.15. *Analysis of neuro-differentiation-promoting activity of CNTs-SS*

BMSCs were seeded in CNTs-SS as the methods described above, and cultured in IMDM containing 10% FBS for 7 or 14 days. The mRNA was extracted from BMSCs by Trizol (Invitrogen, CA, USA) for reverse transcription. Quantitative Real-Time PCR (qRT-PCR) was performed using ThermoScript RT-PCR System (Invitrogen, CA, USA). To examine cell morphology, the BMSCs cultured in the scaffolds for 14 days were stained with Calcein-AM (Biovision, CA, USA) according to the manufacturer's instructions. The BMSCs in the scaffolds were observed using a confocal laser microscope (Nikon A1Si, Japan). A portion of BMSCs in the scaffolds were fixed with 2.5% glutaraldehyde and imaged by scanning electron microscopy (SEM).

The Western blot analyses were performed as previously described [21]. Briefly, the samples were subjected to SDS-PAGE electrophoresis and then transferred to nitrocellulose membranes. After the membranes were incubated with the antibodies: anti-Tuj1 antibody (Ab52623, Abcam, MA, USA) and anti-GAPDH antibody (AC002, Abclonal, Wuhan, China), the blots were examined using a Luminescent Image Analyzer (Fujifilm LAS-4000, Tokyo, Japan). The immunofluorescence staining assay was performed as previously described [21]. The BMSCs cultured in the scaffolds for 14 days were fixed with 4% paraformaldehyde (*w/v*, PBS). The cells were incubated with the antibodies: anti-Tuj1 antibody (Ab52623, Abcam, MA, USA) and a fluorescein (FITC)-conjugated secondary antibody (111-095-003, Jackson ImmunoResearch, PA, USA). The cells were imaged using a confocal laser microscope (Nikon A1Si, Japan).

The BMSCs were transduced with the pTuj1-mCherry vector using Lipofectamine 2000 (Thermo Fisher Scientific, MA, USA). Then the cells were seeded in CNTs-SS. After being cultured for 14 days, the BMSCs were digested from the scaffolds and sorted by a flow cytometer. The GFP-Cherry double positive cells were collected and frozen in liquid

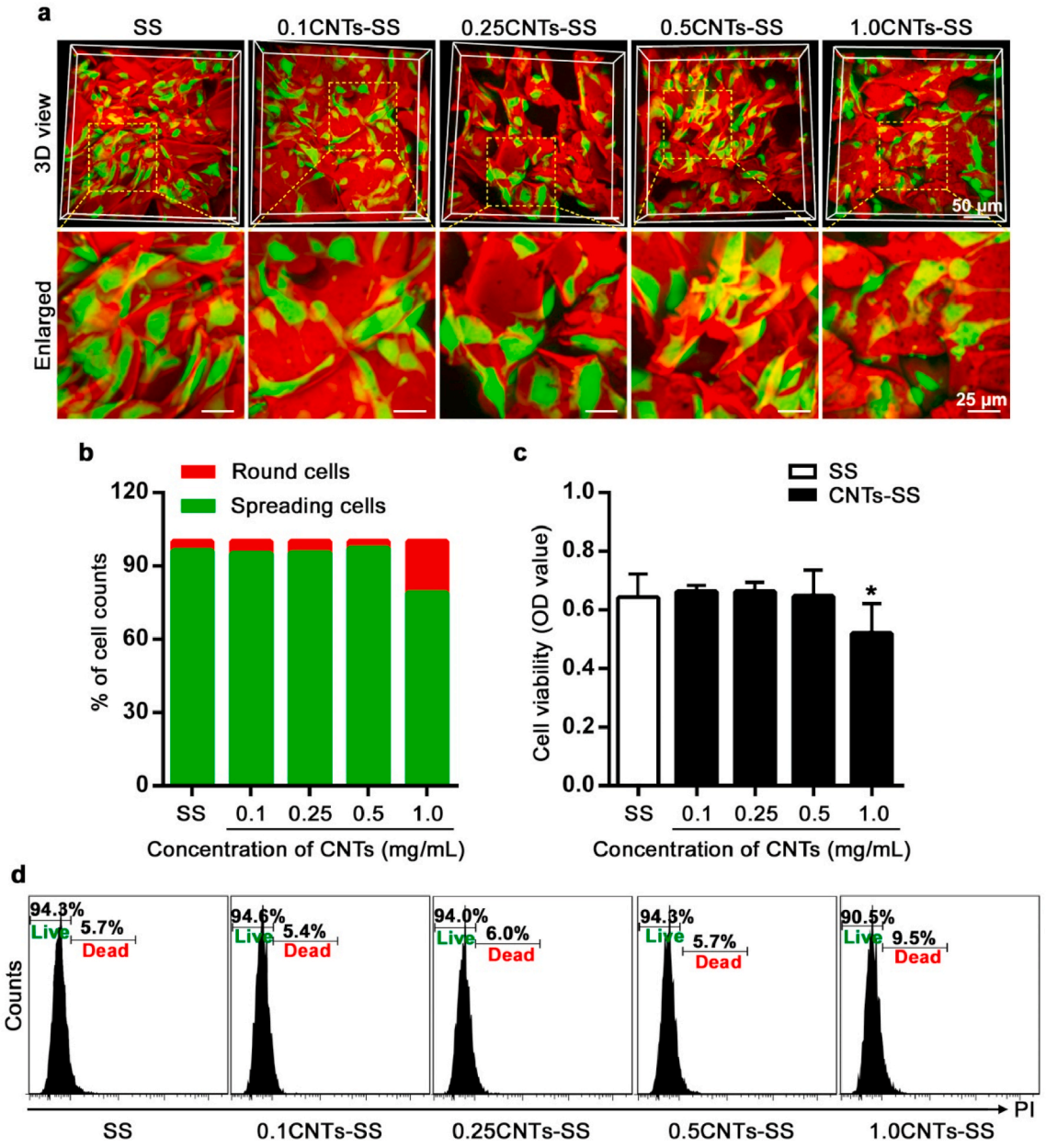

Fig. 2. The neuronal cyto-compatibility of CNTs-SS. (a) The confocal images of GFP-expressing SHSY-5Y cells (green) cultured in SS (red) or CNTs-SS (red) for 3 days. The regions boxed with yellow dashed lines were enlarged in the lower panels. (b) Quantification of the percentages of spreading cells and round cells in (a). (c) The CCK-8 assay for determining cell viability of SHSY-5Y cells cultured in SS or CNTs-SS for 3 days. *, $P < 0.05$; ANOVA. (d) Flow cytometry analyses after Live&Dead cell staining were performed to assess cell viability of SHSY-5Y cells cultured in SS or CNTs-SS for 3 days. (For interpretation of the references to color in this figure legend, the reader is referred to the Web version of this article.)

nitrogen for transportation. The samples' quality control, RNA sequencing and gene expression analysis were carried out in Beijing Genomics Institute (BGI, China). Then, the hierarchical clustering analysis of 40 neuron-associated genes was performed as previously reported [27].

2.16. Statistical analysis

Statistically significant differences among groups were detected by one-way analysis of variance (ANOVA). All data were presented as mean ± standard deviation and $P < 0.05$ was considered statistically significant.

3. Results and discussion

3.1. Preparation and characterization of CNTs-SS

Apart from the biocompatibility, low-immunogenicity and biodegradability, sericin-based hydrogel has been proved to support neurons adhesion and growth, and to possess neuroprotective properties [20,21], making it be a promising material for neural tissue repair. Taking advantages of silkworm genetics, we extracted pure sericin from genetic mutant (fibroin-deficient) silkworm cocoons as previously reported (Figure S1a) [20]. The sericin was crosslinked to form sericin hydrogels with the dopant CNTs ultrasonically blended in, followed by lyophilization to generate scaffolds (CNTs-SS) (Figure S1b, S2a-b). Incorporation of CNTs did not affect pore sizes of the scaffolds, as pure sericin

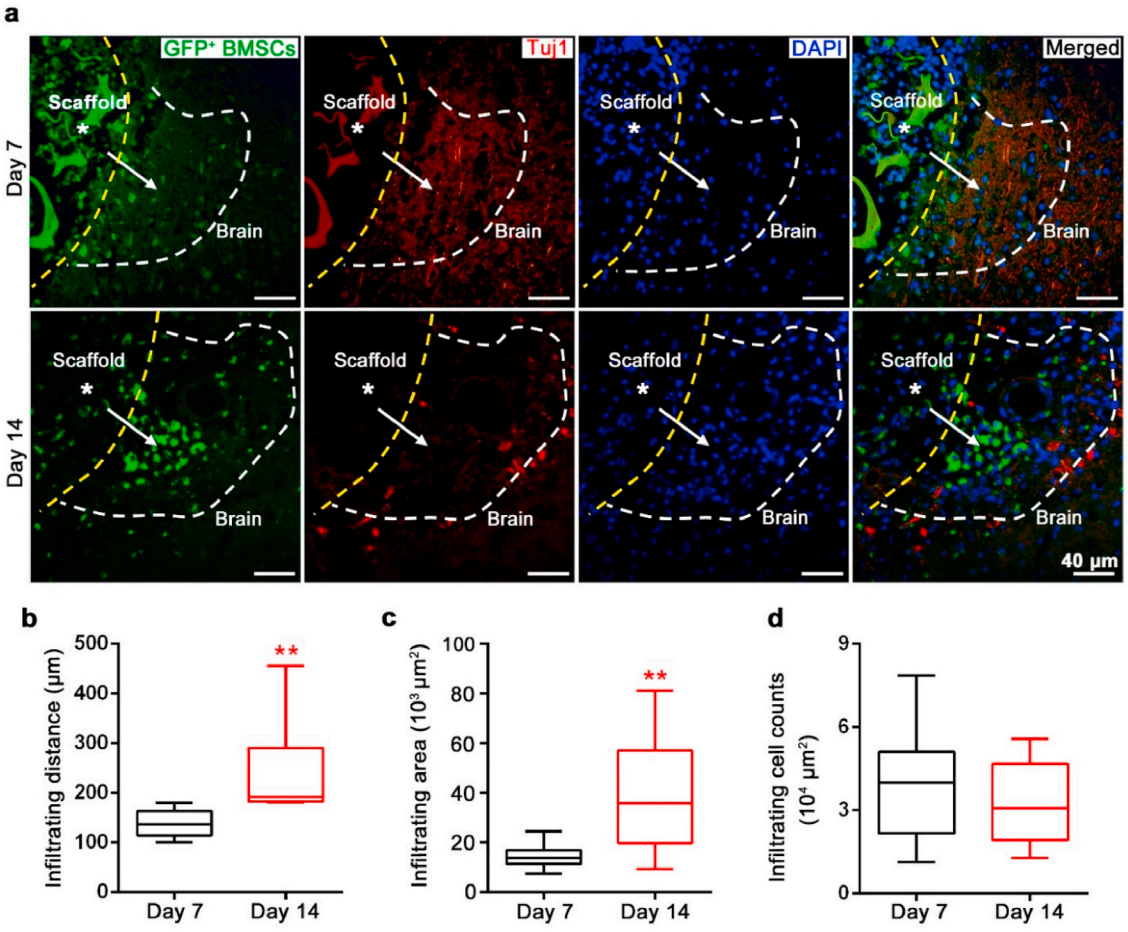

Fig. 3. The CNTs-SS as a cell carrier effectively delivered stem cells to target brain regions. (a) Immunofluorescence staining of the brain sections 7 days or 14 days after brain tissue (Tuj1 positive, red) was implanted with a disk-shaped 0.5CNTs-SS (white asterisks; diameter, 3 mm) carrying GFP-expressing BMSCs (green). Nuclei were stained blue (DAPI). These BMSCs migrated out of the scaffold, crossed the interface (yellow dashed lines) between the scaffold and the brain, and infiltrated into surrounding brain tissue (outlined by white dashed lines). The white arrows indicate BMSC's infiltrating direction. (b–d) Quantification of infiltrating distance (b), infiltrating area (c), and infiltrating cell numbers of GFP-expressing BMSCs (d) after the scaffolds were implanted for 7 days or 14 days. **, $P < 0.01$; N·S·., not significant; Student's *t*-tests. (For interpretation of the references to color in this figure legend, the reader is referred to the Web version of this article.)

scaffold (SS) and CNTs-SS containing 0.5 mg/mL CNTs (0.5CNTs-SS) exhibited similar porous microstructures (Fig. 1a) with the pore diameter of approximately 80 μm (Figure S3a-b). Such pore sizes were thought to facilitate exchange of metabolites and nutrients between scaffolds and microenvironment [28]. As the amount of incorporated CNTs increased, the compressive moduli of CNTs-SS went up from 3.7 kPa to 11.4 kPa (Fig. 1b). Moreover, no significant difference in compressive moduli between the orginal CNTs-SS and the rehydrated CNTs-SS was observed (Figure S4). Given that the compressive moduli of 0.5CNTs-SS and 1.0CNTs-SS were close to that of human brain tissues (11–23 kPa) [29], these two CNTs-SS might provide a bionic physical environment favoring neural tissue regeneration. Moreover, CNTs incorporation also did not affect the swelling properties, as SS and four CNTs-SS scaffolds exhibited similar swelling dynamics: reaching maximal swelling volume (15 times) within the first 48 h (Figure S5) and staying stable (8 days). By inheriting sericin's intrinsic fluorescent property [20,30], 0.5CNTs-SS emitted 750-nm fluorescence (near infrared spectra) when excited by 700-nm light. Such fluorescence was sufficiently strong to enable visual detection of the scaffolds even after being covered by seven layers of murine skin (approximately 5-mm thick) (Fig. 1c). This near-infrared fluorescent property of CNTs-SS would allow *in vivo* detection and noninvasive real-time tracking/monitoring of the scaffold.

3.2. *In vitro cyto-compatibility and in vivo biocompatibility of CNTs-SS*

To determine whether CNTs-SS could act as a cell carrier to effectively support cells' adhesion and proliferation, we generated a GFP-expressing SHSY-5Y neuronal cell line for growing on the scaffolds. 3D reconstruction of confocal images showed that over 85% of neuronal cells directly contacting the scaffolds spread well adopting fusiform morphology (Fig. 2a and b) with cell viability over 90% (Fig. 2c and d). Moreover, CNTs-SS also exhibited good *in vivo* bio-safety and biocompatibility. One and two weeks after a disk-shaped CNTs-SS was implanted onto the brain surface after partial skull removal (Figure S6a), astrocytes and microglia, two main types of inflammation-responding cells in brain, were not functionally activated (no characteristic morphological alterations) (Figure S6b) and not quantitatively increased (Figure S6c). Given that biodegradability of a scaffold is critical for brain regeneration as it would provide additional space for formation of new tissues, we analyzed *in vivo* degradation dynamics of CNTs-SS (Figure S7a-b) and found that the CNTs-SS became structurally loose by Day 28, underwent significant structural dissociation by Day 42 (Week 6), and almost disappeared by Day 56 (Week 8). With the limited regenerative capability, the injured brain tissues would take several months for the differentiation of stem cells and the formation of neuronal networks after the stem cell therapy [31–33]. The 56-day degradation period of CNTs-SS could provide the long-term structural support for the regeneration of *de novo* neural tissues. Moreover, the

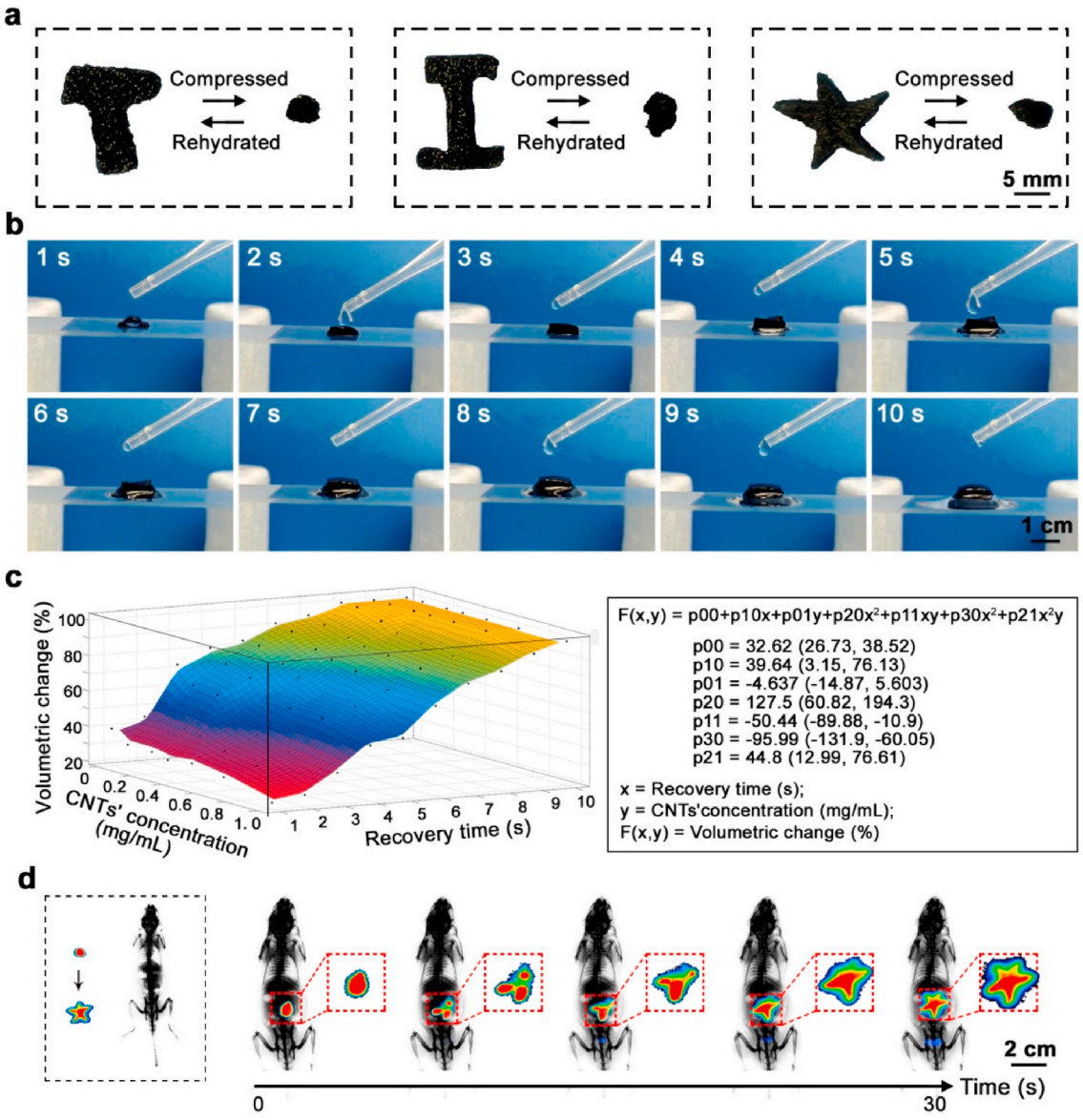

Fig. 4. The shape-memory property of CNTs-SS. (a) The compressed 0.5CNTs-SS in three different shapes recovered to their original shapes after rehydration. (b) Dynamic shape-recovery process of a compressed 0.5CNTs-SS upon rehydration. Frames were extracted from Movie S1. (c) The mathematical model (left) with the corresponding formulation (right) described the programmable recovery behaviors of CNTs-SS. p00, p10, p01, p20, p11, p30 and p21 were coefficients (with 95% confidence bounds); x, y and F (x,y) were three variables as indicated. (d) The compressed 0.5CNTs-SS restored its original pentagram shape after *in vivo* intraperitoneal implantation. Images of implanted scaffolds were enlarged and boxed with red dashed lines. (For interpretation of the references to color in this figure legend, the reader is referred to the Web version of this article.)

degradation of CNTs-SS leaves the addition space for the formation of new tissues, facilitating the brain tissue repair.

3.3. CNTs-SS as an in vivo carrier of stem cells

To investigate if CNTs-SS were capable of delivering cells to target brain regions *in vivo*. GFP-expressing bone marrow mesenchymal stem cells (BMSCs) from GFP transgenic mice were isolated and seeded onto 0.5CNTs-SS. At Day 7 after implantation of the cell-carrying 0.5CNTs-SS onto the brain surface, the GFP-expressing cells delivered by CNTs-SS already migrated out of the scaffold and infiltrated into the neighboring brain tissues (Fig. 3a) by the average depth of 147 μm (Fig. 3b). This migration progressed to the distance of 196 μm at Day 14 (Fig. 3a–b), a 33.3% increase. The average area occupied by infiltrating cells at Day 14 (3.6×10^4 μm^2) was 1.6-time larger than that on Day 7 (1.4×10^4 μm^2) (Fig. 3c). Notably, the total numbers of infiltrating cells were similar between Day 7 (3.9 cells/10^4 μm^2) and Day 14 (3.4 cells/10^4 μm^2) (Fig. 3d), indicating no obvious reduction in the number of living cells, in contrast to rapid cell loss often observed for hydrogels-delivered stem cells [34,35].

Apart from the migration of these exogenous BMSCs, the infiltration of host cells also facilitates the tissue healing [36]. The physically cross-linked hydrogel reportedly supports the infiltration of cells and promotes *in situ* tissue regeneration [37]. The interconnected porous microstructure of CNTs-SS could provide favorable space to support the infiltration of host cells, therefore benefiting the tissue repair. Moreover, give the abundantly active groups of sericin, bioactive factors or inductive factors, such as RGD, N-cadherin peptide, BDNF and TGF-β, could be included in this CNTs-SS through encapsulation or chemical conjugation, promoting cells adhesion (RGD), survival and differentiation [20,38,39], further enhancing the therapeutic outcomes of CNTs-SS.

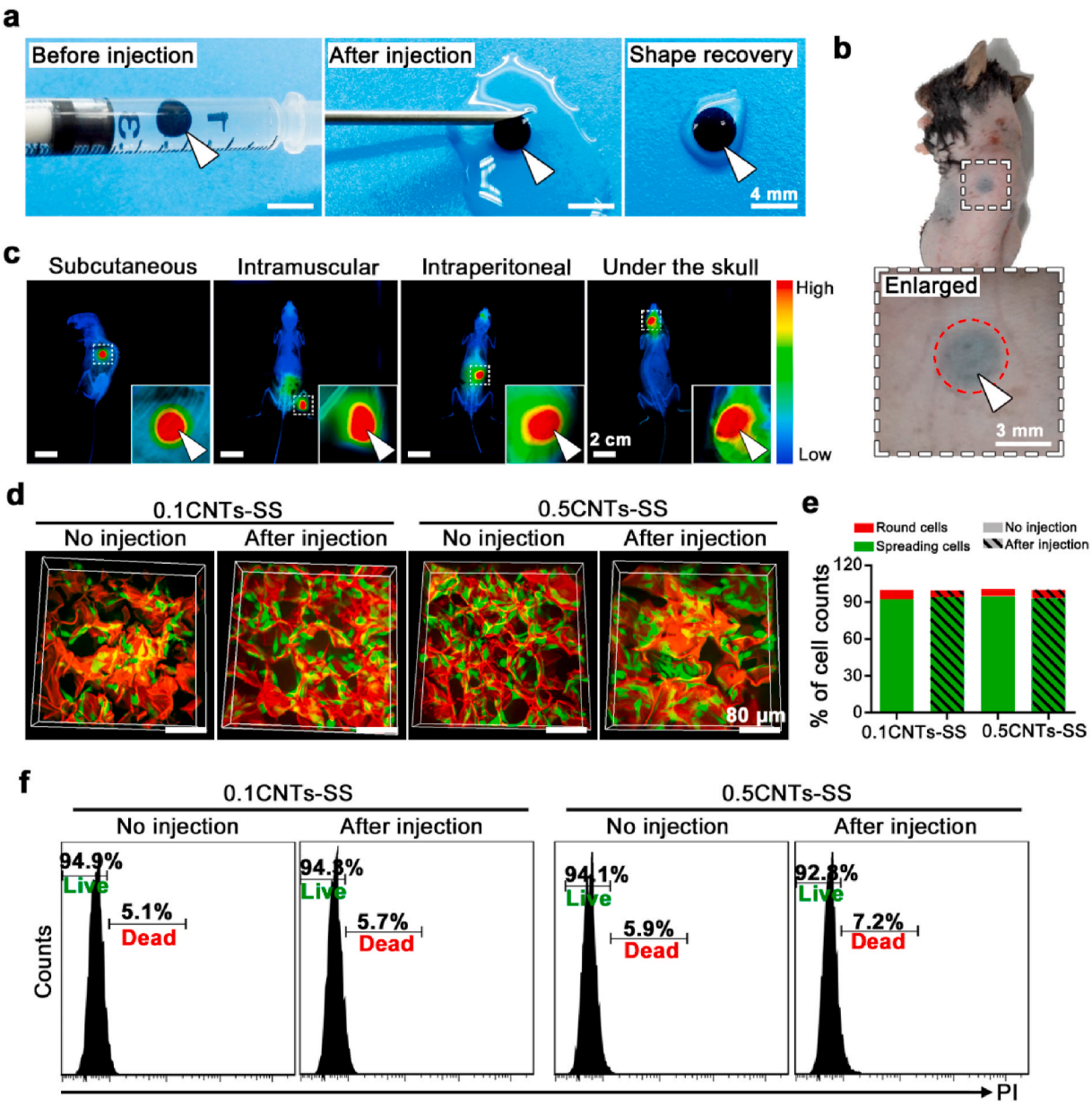

Fig. 5. The injectability of CNTs-SS. (a) Photographs showed that a disk-shaped 0.5CNTs-SS (white arrowheads) in a 1-mL syringe (before injection) was injected through a 16G needle (after injection) and restored its original disk shape (shape recovery). (b) The shape recovery of a disk-shaped 0.5CNTs-SS (white arrowhead; red dashed lines) after subcutaneous injection. The region boxed by white dashed lines was enlarged on the lower panel. (c) Fluorescent images of a disk-shaped 0.5CNTs-SS (white arrowheads) after being injected underneath skin and into muscle, abdomen or brain (excitation 700 nm; emission 750 nm). The regions boxed with white dashed lines were enlarged at the lower right corner. (d) The confocal images of GFP-expressing SHSY-5Y cells (green) carried by CNTs-SS (red) that were injected (After injection) or not injected (No injection). (e) Quantification of the percentages of spreading cells and round cells from the indicated groups in (d). (f) Flow cytometry analysis on cell viability of Live&Dead stained SHSY-5Y cells carried by 0.1CNTs-SS or 0.5CNTs-SS that was injected (After injection) or not injected (No injection). (For interpretation of the references to color in this figure legend, the reader is referred to the Web version of this article.)

3.4. The programmable shape-memory property of CNTs-SS

Unexpectedly, we found that CNTs-SS possessed a shape-memory property. 0.5CNTs-SS with four different shapes ("T", "I", pentagram, and cube shapes) could be volumetrically compressed by roughly 90% into small masses that then restored their original shapes within 10 s upon rehydration (Fig. 4a and b; Table S2; Movie S1). We established a mathematical model to describe the quantitative relations across CNTs' concentrations, recovery time, and volumetric changes via polynomial binary cubic forms (Fig. 4c). In the model, at a given CNTs' concentration, compressed CNTs-SS within a fixed time (10s) (Fig. 4c) appeared to have a fast recovery phase followed by a relatively slow recovery phase. As CNTs' concentrations were elevated, (1) the fast recovery phase was progressively extended, while the slow phase was shortened; (2) the recovery rates (slopes of the curves) in the fast phase were gradually reduced, but were increased in the slow phase. Using this model (Fig. 4c), the recovery behaviors of CNTs-SS could be conveniently programmed by varying its CNTs' concentrations. Since the overly rapid shape restoration of a scaffold would cause rather strong extrusion pressure to damage surrounding normal brain tissues, it is ideal to have restoration dynamics precisely controlled. Aided by this model, we could design a scaffold with on-demand restoration dynamics towards optimizing extrusion pressure during shape recovery. Next, we examined *in vivo* realization of shape-memory property by time-lapse imaging

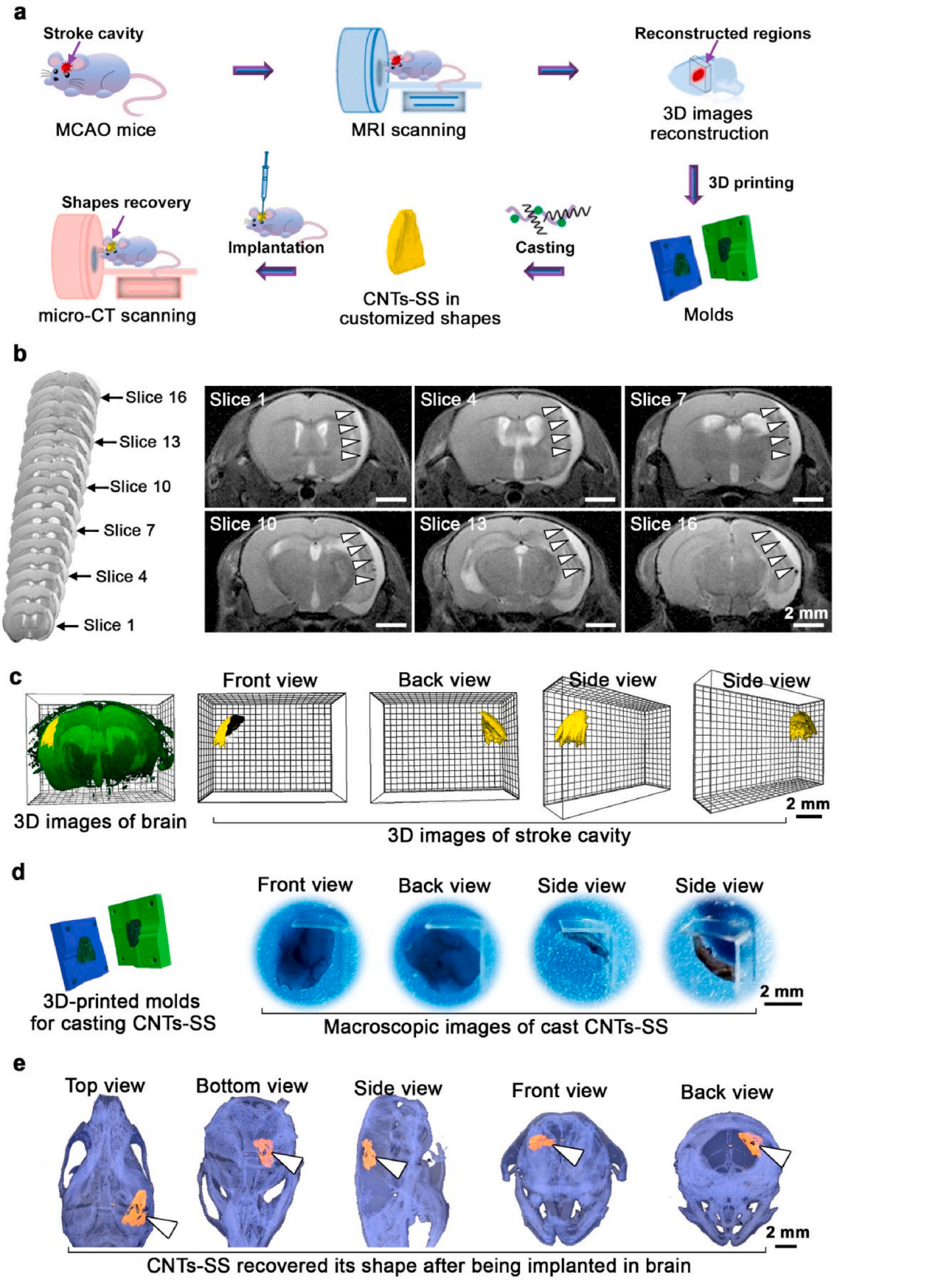

(caption on next page)

Fig. 6. The *in vivo* application of a shape-customized CNTs-SS for filling a random stroke cavity. (a) Schematics showing the whole process of this application: extraction of image information of a stroke cavity in a MCAO mouse for 3D image reconstruction, fabrication of a customized CNTs-SS using a 3D-printed mold, and assessment of its shape recovery after being injected into the cavity. (b) The continuous MRI image series (left) covering the MCAO mouse's brain. Six representative slices from these MRI images showed the site and shape of the stroke cavity (white arrowheads). (c) The 3D reconstruction (left) of MRI images of the MCAO mouse's full brain (green) with the volumetrically-rendered stroke cavity (yellow). The images were extracted from Movie S4. (d) The 3D-printed mold (left) for casting the CNTs-SS with the customized shape geometrically matching the cavity. The newly cast CNTs-SS (right) was viewed from the different angles. (e) The micro-CT images of the injected CNTs-SS (orange; white arrowheads) within the stroke cavity in the brain (skull, light blue) viewed from different angles. The images were extracted from Movie S5. The implanted 0.5CNTs-SS was mixed with 0.1% $BaSO_4$ during fabrication for micro-CT imaging. (For interpretation of the references to color in this figure legend, the reader is referred to the Web version of this article.)

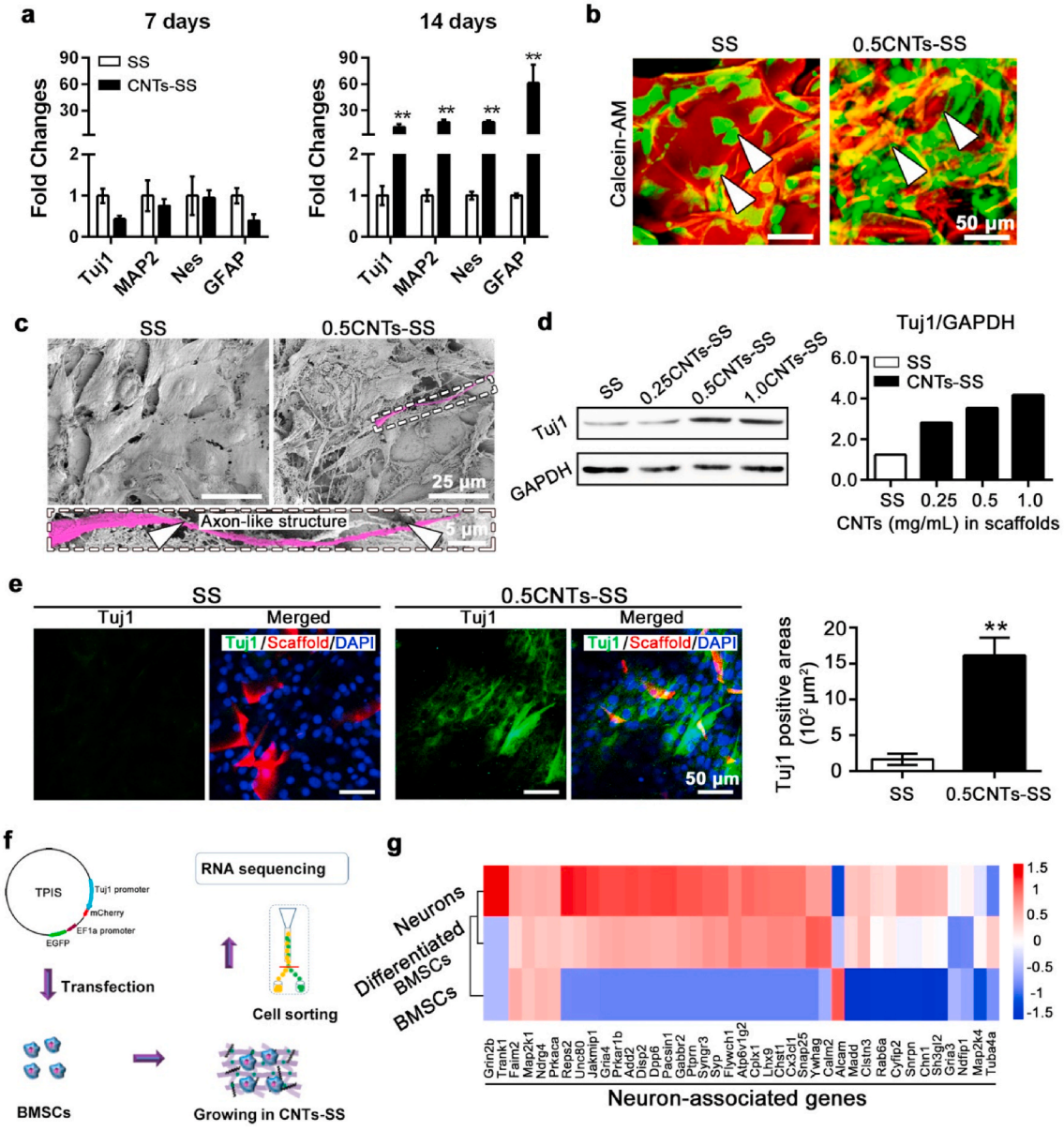

Fig. 7. CNTs-SS promotes BMSCs' neuronal differentiation. (a) The relative mRNA levels of several neuron-associated genes in BMSCs cultured in 0.5CNTs-SS for 7 days or 14 days. **, $P < 0.01$; Student's *t*-tests. (b) The Calcein-AM staining (live-cell morphology; green) of the BMSCs (white arrowheads) with fusiform morphology cultured in SS (left) and the BMSCs with elongated morphology cultured in 0.5CNTs-SS (right) for 14 days. (c) The SEM images of BMSCs cultured in SS (left) or 0.5CNTs-SS (right) for 14 days. The region boxed with white dashed lines was enlarged in the lower panel to show BMSCs' axon-like structure (magenta pseudocolor; white arrowheads). (d) The protein expression of Tuj1 in BMSCs cultured in a series of CNTs-SS for 14 days was analyzed using western blot assay (left), and the corresponding band intensity ratios of Tuj1 to GAPDH were quantified (right). (e) Immunofluorescence staining for Tuj1 (green) in BMSCs (DAPI, blue) cultured in SS (left panel) or 0.5CNTs-SS (right panel) for 14 days. Tuj1 positive area was quantified accordingly (right). **, $P < 0.01$; Student's *t*-tests. (f) Schematics showing the strategy for isolating neuro-differentiated BMSCs for RNA sequencing. The steps include TPIS (Tuj1 Promoter Imaging System, a plasmid system) transfection into BMSCs, cells growing in 0.5CNTs-SS, $TPIS^+$ BMSCs sorting by flow cytometry, and RNA sequencing on sorted $TPIS^+$ BMSCs. (g) The heatmap spectrum representation of mRNA expression of 40 neuron-associated genes in neurons (primary cortical neurons), differentiated BMSCs, and wild-type BMSCs. Hierarchical clustering of the 40 genes transcript profiles of these three types of cells was analyzed. (For interpretation of the references to color in this figure legend, the reader is referred to the Web version of this article.)

the fluorescence emitted from a pentagram-shaped 0.5CNTs-SS. This scaffold was compressed and implanted into the abdominal cavity of a mouse, and successfully recovered to its original shape (Fig. 4d). The sericin's α-helices, that are arranged in coiled-coil architectures, undergo continuous structural transition into metastable β-sheets when load is applied [40], and this reversible transition could be restored in response to hydration, probably endowing the shape-memory properties to CNTs-SS.

Supplementary data related to this article can be found at https://doi.org/10.1016/j.bioactmat.2020.12.017.

3.5. The injectability of CNTs-SS

Similar to water-responsive shape-memory materials (such as methacrylated alginate scaffolds and glycidyl methacrylate functionalized chitosan cryogels) that reportedly have injectability [15,41,42], CNTs-SS were also injectable. The disk-shaped or square-shaped 0.5CNTs-SS in 300 μL phosphate buffer saline (PBS) was readily injected through a conventional 16G needle (Fig. 5a; Movie S2) with no obvious structural destruction detected (Figure S9a-c). Further, several sterile disk-shaped 0.5CNTs-SS suspended in 300 μL PBS were injected into different sites of mice, including skin, muscle, abdomen and brain, and effectively recovered to their original disk shapes (Fig. 5b and c), indicating CNTs-SS′ *in vitro* and *in vivo* injectability. Moreover, CNTs-SS could well protect cells from compressive damage of injection process, which might lead to certain-level microscopic collapse of scaffolds' polymeric networks. Both confocal microscopy and flow cytometry analyses revealed that 92% of GFP-expressing SHSY-5Y cells carried by 0.1CNTs-SS and 0.5CNTs-SS scaffolds remained viable after injection (Fig. 5d–f). This cell protective effect was presumably attributable to extensive connection of pores and physical flexibility of polymeric networks.

Supplementary data related to this article can be found at https://doi.org/10.1016/j.bioactmat.2020.12.017.

3.6. CNTs-SS as customizable scaffolds precisely fill stroke cavitary lesion *in vivo*

To test whether injection direction relative to the position of a stroke cavity affected the final orientation of the shape-restored scaffold within the cavity and its shape-fitting performance to the cavity, we conducted *in vitro* polydimethylsiloxane (PDMS) "stroke" cavity implantation experiments (Figure S10a). Independent of the various orientations of injection needles relative to the PDMS cavity, the compressed scaffold was able to effectively restore its original shape and well fit the cavity (Figure S10b-d). Next, we determined whether CNTs-SS could be precisely and geometrically fill stroke cavity *in vivo* as pre-designed in a mouse stroke model (MCAO) where a middle cerebral artery was occluded (Fig. 6a; Movie S3) [19]. The cavitary lesion in the MCAO mouse was scanned by magnetic resonance imaging (MRI) (Fig. 6b). The stacks of MRI image slices were 3D reconstructed using threshold segmentation algorithm to obtain the cavitary contour (Fig. 6c; Movie S4). Using a digital light processing (DLP) 3D printer, the customized molds based on this contour were printed for casting a 0.5CNTs-SS precisely matching the cavitary geometry (Fig. 6d). The cast scaffold was then intracranially injected into the cavity of the MCAO mouse that was MRI imaged. The scaffold faithfully restored its pre-cast shape (Fig. 6e; Movie S5), which was verified by micro-CT images. These results collectively exemplify the potential utilization of CNTs-SS by showing how CNTs-SS can be morphologically fabricated on demand, minimal-invasively implanted *in vivo*, and geometrically fit an irregular-shaped cavitary lesion, thus demonstrating the feasibility of using CNTs-SS for *in vivo* stroke repair.

Supplementary data related to this article can be found at https://doi.org/10.1016/j.bioactmat.2020.12.017.

3.7. CNTs-SS promote neuronal differentiation of BMSCs

Consistent with CNTs' reportedly neuro-differentiation-promoting activity [22–24], we found that mRNA levels of neuron-associated genes, including neuron-specific class III β-tubulin (Tuj1), microtubule-associated protein 2 (MAP2), nestin (Nes), and glial fibrillary acidic protein (GFAP), were dramatically increased in BMSCs growing in 0.5CNTs-SS at Day 14 (Fig. 7a). These cells developed a highly elongated neuronal morphology (Fig. 7b) with axon-like subcellular structures (0.6 μm in diameter) observed using scanning electron microscopy (SEM) (Fig. 7c). These suggest that BMSCs in the scaffold undergo neuronal differentiation. Supporting this notion, Tuj1's protein levels and the number of Tuj1 positive cells were significantly increased (Fig. 7d and e). Such CNTs-SS′ neuro-differentiation-promoting effect was independently verified in another neural stem cell line (C17.2 cells) (Figure S11a-b), indicating that this effect is not cell-type specific. By transducing BMSCs with a Tuj1 promoter imaging system (TPIS, a plasmid system) where the expression of mCherry fluorescent protein was driven by Tuj1 promoter (Fig. 7f), we sorted and isolated $TPIS^+$ BMSCs alive using flow cytometry and performed RNA sequencing on them (Fig. 7f). The hierarchical clustering analysis revealed that $TPIS^+$ BMSCs with the high-level expression of a set of 40 neuron-associated genes (Table S1) were transcriptomically close to primary neurons but not wild-type BMSCs (Fig. 7g). Thus, BMSCs growing in CNTs-SS scaffolds effectively differentiate towards neurons.

4. Conclusion

In summary, we fabricated a carbon-nanotubes-doped sericin scaffold (CNTs-SS) for stroke repair, which possess programmable shape-memory property, injectability, photoluminescence, and the capability of promoting BMSCs' neuronal differentiation. By combining materials characterizations, mathematical modeling, cell-biological data, imaging techniques and computational 3D reconstruction, 3D printing and casting, molecular and genetic data, as well as stroke animal models, our work presented compelling evidence demonstrating the feasibility and potentiality of implanting a shape-memory, neuro-differentiation-promoting scaffold into stroke cavities for treating a severe ischemic stroke *in vivo*. Thus, our CNTs-SS offers a new type of shape-memory materials with clinical translational potential for personalized brain tissue repair.

CRediT authorship contribution statement

Jian Wang: Conceptualization, Methodology, Investigation, Writing - original draft. **Xiaolin Li:** Software, Resources, Investigation. **Yu Song:** Writing - review & editing, Visualization. **Qiangfei Su:** Formal analysis, Resources. **Xiakeerzhati Xiaohalati:** Data curation. **Wen Yang:** Validation. **Luming Xu:** Resources. **Bo Cai:** Methodology. **Guobin Wang:** Conceptualization, Supervision, Funding acquisition. **Zheng Wang:** Conceptualization, Supervision, Writing - review & editing, Project administration, Funding acquisition. **Lin Wang:** Conceptualization, Supervision, Writing - review & editing, Project administration, Funding acquisition.

Declaration of competing interest

The authors declare no conflict of interest.

Acknowledgements

J.W. and X.L. contributed equally to this work. This work was supported by the National Key Basic Research Program of China [2015CB5540007], the National Natural Science Foundation of China [81671904, 81572866, 81773104, and 81873931], the Science and Technology Program of Chinese Ministry of Education [113044A], the

Major Scientific and Technological Innovation Projects in Hubei Province [2018ACA136], the Integrated Innovative Team for Major Human Diseases Program of Tongji Medical College of HUST, and the Academic Doctor Supporting Program of Tongji Medical College of HUST.

Appendix A. Supplementary data

Supplementary data related to this article can be found at https://doi.org/10.1016/j.bioactmat.2020.12.017.

References

[1] L. Catanese, J. Tarsia, M. Fisher, Acute ischemic stroke therapy overview, Circ. Res. 120 (3) (2017) 541–558.
[2] A.A. Neuhaus, Y. Couch, G. Hadley, A.M. Buchan, Neuroprotection in stroke: the importance of collaboration and reproducibility, Brain 140 (8) (2017) 2079–2092.
[3] H. Ghuman, C. Mauney, J. Donnelly, A.R. Massensini, S.F. Badylak, M. Modo, Biodegradation of ECM hydrogel promotes endogenous brain tissue restoration in a rat model of stroke, Acta Biomater. 80 (2018) 66–84.
[4] M.V. Sofroniew, H.V. Vinters, Astrocytes: biology and pathology, Acta Neuropathol. 119 (1) (2010) 7–35.
[5] E. Bible, D.Y. Chau, M.R. Alexander, J. Price, K.M. Shakesheff, M. Modo, The support of neural stem cells transplanted into stroke-induced brain cavities by PLGA particles, Biomaterials 30 (16) (2009) 2985–2994.
[6] E. Bible, O. Qutachi, D.Y. Chau, M.R. Alexander, K.M. Shakesheff, M. Modo, Neovascularization of the stroke cavity by implantation of human neural stem cells on VEGF-releasing PLGA microparticles, Biomaterials 33 (30) (2012) 7435–7446.
[7] L.R. Nih, S. Gojgini, S.T. Carmichael, T. Segura, Dual-function injectable angiogenic biomaterial for the repair of brain tissue following stroke, Nat. Mater. 17 (7) (2018) 642–651.
[8] J. Lam, W.E. Lowry, S.T. Carmichael, T. Segura, Delivery of iPS-NPCs to the stroke cavity within a hyaluronic acid matrix promotes the differentiation of transplanted cells, Adv. Funct. Mater. 24 (44) (2014) 7053–7062.
[9] H.X. Zhang, F. Sun, J.X. Wang, L.K. Xie, C.Q. Yang, M.X. Pan, B. Shao, G.Y. Yang, S. H. Yang, Q.C. ZhuGe, K.L. Jin, Combining injectable plasma scaffold with mesenchymal stem/stromal cells for repairing infarct cavity after ischemic stroke, Aging Dis 8 (2) (2017) 203–214.
[10] K. Jin, X. Mao, L. Xie, V. Galvan, B. Lai, Y. Wang, O. Gorostiza, X. Wang, D. A. Greenberg, Transplantation of human neural precursor cells in Matrigel scaffolding improves outcome from focal cerebral ischemia after delayed postischemic treatment in rats, J. Cerebr. Blood Flow Metabol. 30 (3) (2010) 534–544.
[11] N.J. Darling, E. Sideris, N. Hamada, S.T. Carmichael, T. Segura, Injectable and spatially patterned microporous annealed particle (MAP) hydrogels for tissue repair applications, Adv. Sci. 5 (11) (2018).
[12] J. Whitehead, K. Bolland, E. Valdes-Marquez, A. Lihic, M. Ali, K. Lees, V. Collaborators, Using historical lesion volume data in the design of a new phase II clinical trial in acute stroke, Stroke 40 (4) (2009) 1347–1352.
[13] A.E. Baird, A. Benfield, G. Schlaug, B. Siewert, K.O. Lovblad, R.R. Edelman, S. Warach, Enlargement of human cerebral ischemic lesion volumes measured by diffusion-weighted magnetic resonance imaging, Ann. Neurol. 41 (5) (1997) 581–589.
[14] L. Yu, J.D. Ding, Injectable hydrogels as unique biomedical materials, Chem. Soc. Rev. 37 (8) (2008) 1473–1481.
[15] S.A. Bencherif, R.W. Sands, D. Bhatta, P. Arany, C.S. Verbeke, D.A. Edwards, D. J. Mooney, Injectable preformed scaffolds with shape-memory properties, Proc. Natl. Acad. Sci. U.S.A. 109 (48) (2012) 19590–19595.
[16] M. Spector, T.C. Lim, Injectable biomaterials: a perspective on the next wave of injectable therapeutics, Biomed. Mater. 11 (1) (2016), 014110.
[17] T.M. Bliss, R.H. Andres, G.K. Steinberg, Optimizing the success of cell transplantation therapy for stroke, Neurobiol. Dis. 37 (2) (2010) 275–283.
[18] O. Lindvall, Z. Kokaia, Stem cells in human neurodegenerative disorders–time for clinical translation? J. Clin. Invest. 120 (1) (2010) 29–40.
[19] W. Tu, X. Xu, L. Peng, X. Zhong, W. Zhang, M.M. Soundarapandian, C. Balel, M. Wang, N. Jia, F. Lew, S.L. Chan, Y. Chen, Y. Lu, DAPK1 interaction with NMDA receptor NR2B subunits mediates brain damage in stroke, Cell 140 (2) (2010) 222–234.
[20] Z. Wang, Y. Zhang, J. Zhang, L. Huang, J. Liu, Y. Li, G. Zhang, S.C. Kundu, L. Wang, Exploring natural silk protein sericin for regenerative medicine: an injectable, photoluminescent, cell-adhesive 3D hydrogel, Sci. Rep. 4 (2014) 7064.
[21] Z. Wang, J. Wang, Y. Jin, Z. Luo, W. Yang, H.J. Xie, K. Huang, L. Wang, A neuroprotective sericin hydrogel as an effective neuronal cell carrier for the repair of ischemic stroke, ACS Appl. Mater. Interfaces 7 (44) (2015) 24629–24640.
[22] S.Y. Park, B.S. Kang, S. Hong, Improved neural differentiation of human mesenchymal stem cells interfaced with carbon nanotube scaffolds, Nanomedicine 8 (5) (2013) 715–723.
[23] M.C. Serrano, S. Nardecchia, C. Garcia-Rama, M.L. Ferrer, J.E. Collazos-Castro, F. del Monte, M.C. Gutierrez, Chondroitin sulphate-based 3D scaffolds containing MWCNTs for nervous tissue repair, Biomaterials 35 (5) (2014) 1543–1551.
[24] Y.J. Huang, H.C. Wu, N.H. Tai, T.W. Wang, Carbon nanotube rope with electrical stimulation promotes the differentiation and maturity of neural stem cells, Small 8 (18) (2012) 2869–2877.
[25] M.N. Islam, S.R. Das, M.T. Emin, M. Wei, L. Sun, K. Westphalen, D.J. Rowlands, S. K. Quadri, S. Bhattacharya, J. Bhattacharya, Mitochondrial transfer from bone-marrow-derived stromal cells to pulmonary alveoli protects against acute lung injury, Nat. Med. 18 (5) (2012), 759-U153.
[26] H.B. Liu, T. Huang, M.J. Li, M. Li, C.X. Zhang, J. Jiang, X.C. Yu, Y.Y. Yin, F. Zhang, G. Lu, M.C. Luo, L.R. Zhang, J.S. Li, K. Liu, Z.J. Chen, SCRE serves as a unique synaptonemal complex fastener and is essential for progression of meiosis prophase I in mice, Nucleic Acids Res. 47 (11) (2019) 5670–5683.
[27] Q. Zhao, A. Kho, A.M. Kenney, D.I. Yuk Di, I. Kohane, D.H. Rowitch, Identification of genes expressed with temporal-spatial restriction to developing cerebellar neuron precursors by a functional genomic approach, Proc. Natl. Acad. Sci. U.S.A. 99 (8) (2002) 5704–5709.
[28] H.Q. Cao, T. Liu, S.Y. Chew, The application of nanofibrous scaffolds in neural tissue engineering, Adv. Drug Deliv. Rev. 61 (12) (2009) 1055–1064.
[29] X. Jin, F. Zhu, H.J. Mao, M. Shen, K.H. Yang, A comprehensive experimental study on material properties of human brain tissue, J. Biomech. 46 (16) (2013) 2795–2801.
[30] J. Liu, C. Qi, K. Tao, J. Zhang, J. Zhang, L. Xu, X. Jiang, Y. Zhang, L. Huang, Q. Li, H. Xie, J. Gao, X. Shuai, G. Wang, Z. Wang, L. Wang, Sericin/dextran injectable hydrogel as an optically trackable drug delivery system for malignant melanoma treatment, ACS Appl. Mater. Interfaces 8 (10) (2016) 6411–6422.
[31] L. Binan, A. Ajji, G. De Crescenzo, M. Jolicoeur, Approaches for neural tissue regeneration, Stem Cell Rev. Rep. 10 (1) (2014) 44–59.
[32] B.J. Cummings, N. Uchida, S.J. Tamaki, D.L. Salazar, M. Hooshmand, R. Summers, F.H. Gage, A.J. Anderson, Human neural stem cells differentiate and promote locomotor recovery in spinal cord-injured mice, Proc. Natl. Acad. Sci. U.S.A. 102 (39) (2005) 14069–14074.
[33] J.R. Munoz, B.R. Stoutenger, A.P. Robinson, J.L. Spees, D.J. Prockop, Human stem/progenitor cells from bone marrow promote neurogenesis of endogenous neural stem cells in the hippocampus of mice, Proc. Natl. Acad. Sci. U.S.A. 102 (50) (2005) 18171–18176.
[34] F.G. Yu, C.M. Morshead, Adult stem cells and bioengineering strategies for the treatment of cerebral ischemic stroke, Curr. Stem Cell Res. Ther. 6 (3) (2011) 190–207.
[35] H. Sakata, P. Narasimhan, K. Niizuma, C.M. Maier, T. Wakai, P.H. Chan, Interleukin 6-preconditioned neural stem cells reduce ischaemic injury in stroke mice, Brain 135 (Pt 11) (2012) 3298–3310.
[36] C. Wang, H. Yue, Q. Feng, B. Xu, L. Bian, P. Shi, Injectable nanoreinforced shape-memory hydrogel system for regenerating spinal cord tissue from traumatic injury, ACS Appl. Mater. Interfaces 10 (35) (2018) 29299–29307.
[37] Q. Feng, J. Xu, K. Zhang, H. Yao, N. Zheng, L. Zheng, J. Wang, K. Wei, X. Xiao, L. Qin, L. Bian, Dynamic and cell-infiltratable hydrogels as injectable carrier of therapeutic cells and drugs for treating challenging bone defects, ACS Cent. Sci. 5 (3) (2019) 440–450.
[38] L. Zhang, W. Yang, H.J. Xie, H. Wang, J. Wang, Q.F. Su, X.L. Li, Y. Song, G. B. Wang, L. Wang, Z. Wang, Sericin nerve guidance conduit delivering therapeutically repurposed clobetasol for functional and structural regeneration of transected peripheral nerves, ACS Biomater. Sci. Eng. 5 (3) (2019) 1426–1439.
[39] L. Zhang, W. Yang, K. Tao, Y. Song, H. Xie, J. Wang, X. Li, X. Shuai, J. Gao, P. Chang, G. Wang, Z. Wang, L. Wang, Sustained local release of NGF from a chitosan-sericin composite scaffold for treating chronic nerve compression, ACS Appl. Mater. Interfaces 9 (4) (2017) 3432–3444.
[40] L. Cera, G.M. Gonzalez, Q. Liu, S. Choi, C.O. Chantre, J. Lee, R. Gabardi, M.C. Choi, K. Shin, K.K. Parker, A bioinspired and hierarchically structured shape-memory material, Nat. Mater. (2020), https://doi.org/10.1038/s41563-020-0789-2.
[41] B. Newland, P.B. Welzel, H. Newland, C. Renneberg, P. Kolar, M. Tsurkan, A. Rosser, U. Freudenberg, C. Werner, Tackling cell transplantation anoikis: an injectable, shape memory cryogel microcarrier platform material for stem cell and neuronal cell growth, Small 11 (38) (2015) 5047–5053.
[42] X. Zhao, B. Guo, H. Wu, Y. Liang, P.X. Ma, Injectable antibacterial conductive nanocomposite cryogels with rapid shape recovery for noncompressible hemorrhage and wound healing, Nat. Commun. 9 (1) (2018) 2784.